Electron attachment and quantum coherence in molecular hydrogen

Electron attachment and quantum coherence in molecular hydrogen

Vaibhav S Prabhudesai[1], Nigel J Mason[2] and E Krishnakumar[3]

[1] Tata Institute of Fundamental Research, Homi Bhabha Road, 400005 Mumbai, India
[2] School of Physical Sciences, University of Kent, Canterbury, CT2 7NH, UK
[3] Raman Research Institute, Sadashiva Nagar, 560080 Bengaluru, India

Email: vaibhav@tifr.res.in

Abstract. Single electron attachment to a molecule may invoke quantum coherence in different angular momentum transfer channels. This has been observed in the 14 eV dissociative electron attachment resonance in molecular hydrogen where a coherent superposition of two negative ion resonant states of opposite parity is created, with the *s* and *p* partial waves of the electron contributing to the attachment process. Interference between the two partial wave contributions leads to a forward – backward asymmetry in the angular distribution of the product negative ions. Since these two resonant states dissociate to the same n = 2 state of H and H^-, this asymmetry is further modified due to interference between the two paths of the dissociating molecular negative ion along different potential energy curves. This interference manifests as a function of the electron energy as well as isotopic composition. This case is akin to the quantum interference observed in photodissociation by one-photon vs two-photon absorption.

1. Introduction

Dissociative electron attachment (DEA) is a dominant process in any medium in which low energy electrons are present. It is an efficient way of converting kinetic energy into chemical energy in a medium and has been exploited by modern laser technology and play a role in many planetary and astrophysical phenomena. A major characteristic of the DEA process is its ability to induce site selective bond breaks in molecules [1-4]. It has been shown that electron attachment to molecules depends on the functional groups present in them, leading to localization of both energy and charge at a given site in the molecule [1]. The subsequent dissociation of the molecular negative ion resonance (NIR) state takes place selectively at a given bond or site. Furthermore, since electron attachment occurs at distinct energies and leads to distinct molecular fragmentation pathways, DEA provides a way of controlling the chemistry by controlling the creation of reactive species in a medium. This is complementary to the coherent control of chemical reaction using lasers. However, electrons being ubiquitous, the possibility of chemical control using electrons may have wider applicability than coherent control of chemical reactions using lasers and is a more practical technology. Indeed, it is now being adopted in plasma technology and nanotechnologies [5].

Coherent control using lasers has been used to demonstrate control in photodissociation. In this, the quantum coherence manifests itself in terms of quantum interference of two or more channels that start from an initial state of a target molecule and lead to the same dissociation products. Selection of one of these channels has been demonstrated by controlling the coherent light fields. Breaking of inversion

symmetry in the photodissociation using one photon vs two photon absorption is the most robust example of demonstration of such coherence and its control [6].

In many aspects, the DEA process is very similar to photodissociation. The kinetic energy of the attaching electron is transferred to the target molecule which causes its excitation and this excited state may then undergo dissociation. However, the most distinctive feature of DEA is the transfer of charge which results in the formation of a NIR. Depending on the electron affinity of the fragments, the DEA process invokes additional energy release which makes bond rupture in molecules possible for electron energies even below their dissociation limits. Also, unlike photoabsorption where in the visible frequency regime the dipole transition plays a dominant role, in electron attachment more than one value of angular momentum may be transferred with comparable strength. However, the most intriguing aspect of the DEA process is the rich electron-electron correlations that result due to interaction of the attached electron with those from the molecular target. This makes theoretical calculations of the electron attachment and DEA process more challenging. Experimentally, the DEA process has been studied through measurements of the absolute cross sections of various dissociation channels as well as measurements of the kinetic energy and angular distributions of the fragment anions [7-11]. Fragment kinetic energy distribution yields information about the energy partitioning in the dissociation process whereas angular distribution reflects the NIR state symmetries involved, provided the dissociation takes place on a fast enough time scale. Together such measurements allow modeling of the DEA dynamics.

We have recently observed in molecular hydrogen coherence in electron attachment leading to the formation of two negative ion resonances in coherent superposition and subsequent decay of the system through dissociation [12]. That this process is observed in the simplest molecular system makes it all the more interesting. It may be pointed out that no theoretical prediction or any observation has been made for such a process in any other system before. What we present here is a more detailed analysis of the data and discuss the implications of the results for understanding the NIRs in molecular hydrogen around 14 eV.

2. Negative ion resonances in molecular hydrogen

Before we discuss present results, it is appropriate to give a brief review of the status of negative ion resonances in molecular hydrogen. Being the simplest molecule, electron scattering from H_2 (and its isotopomers) has been the subject of considerable theoretical and experimental work. The NIRs in molecular hydrogen have been observed in DEA studies, electron transmission experiments, elastic and inelastic scattering experiments and various theoretical calculations. All these are summarised in several reviews [11, 13-17]. Recent measurements [18] on absolute cross sections for DEA on H_2 and D_2 have removed the disparity that existed in previous data [19, 20]. The DEA process in the molecule has been shown to have strong isotope effect [18, 19, 21, 22], due to the considerable mass difference in the nuclei. All the isotopomers are also found to have strong initial vibrational state dependence in the DEA cross sections [23, 24]. This has been explained by the combined effect of the Franck– Condon factors and the survival factor appropriate to the calculated potential energy curves [25, 26].

DEA to molecular hydrogen and its isotopomers is characterised by two relatively narrow resonances at 4 eV and 14 eV respectively and a broad one between 7 eV and 13 eV. Based on the measurements and the theoretical calculations [27-29] the symmetries of the three resonances seen in the DEA channel have been assigned as $^2\Sigma_u^+$ (4 eV), $^2\Sigma_g^+$ (10 eV) and $^2\Sigma_u^+$ (14 eV). The H^- angular distribution measurements in DEA at 4 eV and the 10 eV peaks were found to be consistent with these assignments [30]. Preliminary measurements [31] on the H^- angular distribution at 14 eV resonance were found to be isotropic and it was assumed that the symmetry of the resonance was the same as that determined by inelastic electron scattering measurements [32]. However, an interesting feature of measurements of ion yield curves is the observation of oscillation in the energy differential cross sections between 11 eV and 13 eV [31] and between 14 eV and 16 eV [30] for H_2 and the absence of such structures in D_2. No clear explanation has been made for both these structures, though it was proposed that the observed structure between 11 eV and 13 eV may involve an attractive $^2\Sigma_g^+$ NIR either through predissociation or a two-step process [33] in which the resonant elastic scattering from the attractive $^2\Sigma_g^+$ is followed by DEA

through the repulsive $^2\Sigma_g^+$ state [31]. The structure in the 14 eV resonance was proposed as due to predissociation from a $^2\Delta_g$ state where the coupling takes place through rotations [30]. Since there is a requirement of unit angular momentum change between the two states in the predissociation process, Tronc *et al.* [30] proposed a breakdown of Born-Oppenheimer approximation with the Δ_g state having a dissociation limit of $H^-(1s^2)$ + H(3d) which is bound in the relevant electron energy range.

3. Experimental set-up

We have used the velocity slice imaging (VSI) technique [18, 34] to measure the angular distribution of the fragment anions produced in the DEA to H_2. In brief, an effusive molecular beam crosses a magnetically collimated pulsed electron beam at right angle. The molecular beam is coincident with the axis of the VSI spectrometer. The spectrometer consists of the interaction region followed by a single element electrostatic lens and 100mm long flight tube. The ions are detected using micro channel plates and phosphor screen-based position sensitive detector (PSD). The ions formed in the interaction region are extracted using a delayed pulsed electric field applied to the extraction electrodes. The electrostatic lens assembly provides the velocity focusing condition where the entire Newton sphere of the extracted fragment anions is projected onto the 2-dimensional PSD. The detector is subjected to an 80nsec wide voltage pulse, which is timed appropriately coinciding with the arrival of the central slice of the Newton sphere. The impacts of the ions on the detector are recorded using CCD camera and analyzed after adding several such slices in an off-line analysis. The energy resolution of the electron beam in the experiment is about 0.6 eV. The angular resolution depends on the electron energy and the collimating magnetic field strength as discussed in detail previously [34]. We estimate that it is close to 8° at 4 eV and 4° at 14 eV for a magnetic field of 50 Gauss used in the present measurements.

4. Results

Of the three resonances in H_2, the present discussion is focused upon the 14 eV resonance. We have obtained VSI images of H^- produced from H_2 and D^- from D_2 at a number of electron energies across this resonance. For comparison we have also measured the momentum images around the 4 eV resonance in H_2.

4.1. 4 eV resonance

The 4eV peak in DEA to H_2 is known to be due to ground NIR state of H_2^-. The momentum image obtained at 4.5 eV along with the angular distribution obtained from the image is shown in figure 1.

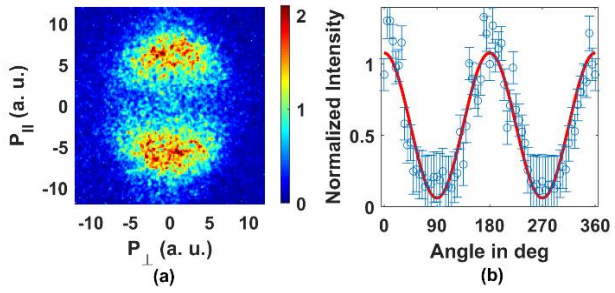

Figure 1. (a) Momentum image obtained for H^- from H_2 at 4.5 eV electron energy. (b) Angular distribution (normalized at θ = 180°) obtained from the image. Measured data (circles) and the fitted distribution (solid line). (Part (a) is reproduced from figure 3(a) of reference 12).

The ion signal peaks symmetrically in forward and backward directions with respect to the incoming electron beam. As the kinetic energy release is low for this resonance, the angular distribution was obtained from the outer edge of the momentum image. The angular distribution follows the $\cos^2\theta$ form with constant background. The exact fit function is of the form,

$$I(\theta) = A^2 + B^2\cos^2(\theta) \quad (1)$$

with A = 0.2457 and B = 1.01. This is consistent with the transition to a NIR state of Σ_u symmetry from the target state of Σ_g symmetry. The dominant angular momentum transfer channel is l = 1 which is the lowest allowed partial wave for this transition in a homonuclear diatomic molecule. Ideally, the value

of *A* should be zero. In the present case, it appears as due to a small background signal and imperfections in the momentum imaging. This background, which can be ignored in this case, becomes a limitation in the analysis of the 14 eV resonance, as will be seen later. We could not measure the D^- angular distribution at this energy due to its two orders of magnitude lower cross section [20].

4.2. 14 eV resonance

The VSI image obtained at 14.5 eV for both H_2 and D_2 along with the angular distributions are shown in figure 2. As can be seen from the figure, the H^- momentum image shows a clear forward-backward asymmetry with respect to the electron beam with more intensity in the backward direction. The VSI image of D^- from D_2 shows substantially different distribution with a different degree of asymmetry.

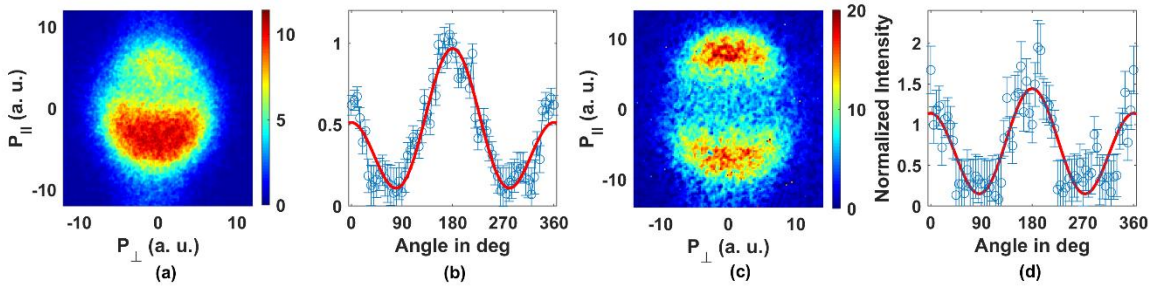

Figure 2. (a) Momentum image and (b) angular distribution (circles - measured data and solid line fit) for H^- from H_2 at 14.5eV electron energy and that ((c) and (d) respectively) for D^- from D_2. The angular distribution is normalized with respect to the count at $\theta = 180^0$. For the details of the fit, please see the text below. (Parts (a) and (c) are reproduced from figure 3(b) and (f) of reference 12).

5. Discussion

5.1. Manifestation of quantum coherence in DEA

For homonuclear diatomic molecules, due to the inversion symmetry present in the system, the dissociation process resulting from a given NIR state must also show inversion symmetry. As the initial neutral target state and the anion state formed after electron attachment has the inversion symmetry, the electron attachment must proceed with transfer of only odd or only even partial waves to the target [35]. The angular distribution thus obtained is given as

$$\mathrm{I}(k,\theta,\phi) = \left|\sum_{l=|\mu|}^{\infty} a_{l\mu}(k)\mathrm{Y}_{l\mu}(\theta,\phi)\right|^2 \quad (2)$$

where *l* has either only odd or only even values. As the target neutral state of H_2 is with even parity, the transfer of even partial wave will result in the formation of NIR with even parity and that of odd partial wave will generate an odd parity NIR state. Consequently, a single NIR state cannot explain the observed forward-backward asymmetry of the angular distribution where the inversion symmetry of the system is broken. However, if we have more than one resonance taking part in the electron attachment, the angular distribution of the product ion is given by

$$\mathrm{I}(k,\theta,\phi) = \sum_{|\mu|}\left|\sum_{l=|\mu|}^{\infty} a_{l\mu}(k)\mathrm{Y}_{l\mu}(\theta,\phi)\right|^2. \quad (3)$$

Please note that here the individual cross sections for each resonant state are simply added and will not break the inversion symmetry. A single electron on attachment creates one resonant state with a certain probability and in an ensemble it is possible to get different states by different electrons. The resultant observable angular distribution will be an incoherent addition of these signals. However, if a single electron upon attachment gives rise to a coherent superposition of different resonant states, the resultant angular distribution stems from the coherent addition of transition amplitudes for dissociation via each constituent state. In this case, the angular distribution will be given by

$$\mathrm{I}(k,\theta,\phi) = \left|\sum_{|\mu|} \sum_{l=|\mu|}^{\infty} a_{l\mu}(k)\mathrm{Y}_{l\mu}(\theta,\phi)\right|^2. \quad (4)$$

For example, in the case of H_2, considering only the lowest order allowed partial waves (angular momentum transfer) in the formation of coherent superposition of $^2\Sigma_g^+$ and $^2\Sigma_u^+$ states from the neutral ground state ($^1\Sigma_g^+$), we can write this equation as

$$\mathrm{I}(k,\theta,\phi) = |a_{00}(k)\mathrm{Y}_{00}(\theta,\phi) + a_{10}(k)\mathrm{Y}_{10}(\theta,\phi)|^2. \quad (5)$$

Based on this, the functional form of the electron attachment probability with respect to angle will be

$$\mathrm{I}(k,\theta) = (a_g(k))^2 + (a_u(k))^2\cos^2\theta + 2a_g(k)a_u(k)\cos\theta\cos\delta \quad (6)$$

where a_g and a_u are proportional to the magnitude of the two transition amplitudes to the $^2\Sigma_g^+$ and $^2\Sigma_u^+$ NIR states respectively with δ as the relative phase between the transferred *s* and *p* waves. From this, one can immediately see that due to the cosθ term there will be a forward-backward asymmetry.

In the present experiment what we observe is the decay of this state through dissociation and under the axial recoil approximation the angular distribution in the attachment probability will manifest itself in the angular distribution of the H^- fragment. However, this by itself does not explain the observed results and we need to consider the evolution of the coherent states leading to dissociation. As the resonances progress towards the dissociation limit along two different potential energy curves, the phase between the two changes and, at the dissociation limit, there will be a phase difference between the two. This phase difference modifies the angular distribution as,

$$\mathrm{I}(k,\theta) = A_g{}^2 + A_u{}^2\cos^2\theta + 2A_gA_u\cos\theta\cos\varphi \quad (7)$$

where A_g and A_u are the amplitudes of each resonant state at the dissociation limit after taking into account the respective autodetachment rate, which is a function of the inter-nuclear separation. We will discuss this point later. The phase φ is the sum of δ (equation (6)) and the phase difference arising from the propagation of the wavepacket along the two dissociation paths. As can be seen from equation (7), the extent of asymmetry observed in the differential cross section will explicitly depend on the relative phase between the two paths that contribute to the DEA channel as well as on the relative amplitudes in the two paths.

The observed difference in asymmetry in D_2 can then be understood as a manifestation of both the change in phase difference as well as change in relative contribution of the two paths. D_2 being a heavier molecule, the dissociation time would be $\sqrt{2}$ times longer than that in H_2. This will change the phase difference between two paths by a factor $\sqrt{2}$ resulting in a change in the interference intensity. On the other hand, each NIR state during dissociation competes with the autodetachment and the lifetime of this process varies as a function of inter-nuclear distance resulting in its survival probability as

$$\mathrm{p_i} = \int_{R_c}^{R_\varepsilon} \frac{\Gamma_a(R)}{\hbar v(R)}\mathrm{d}R = \int_{t_{R_c}}^{t_{R_\varepsilon}} \frac{\mathrm{d}t_R}{\tau(t_R)} \quad (8)$$

where $\Gamma_a(R)$ is the width of the anion potential energy curve, $v(R)$ is the speed of separation of the dissociating atoms, R_c is the inter-nuclear separation at which electron capture takes place and R_ε is the effective inter-nuclear separation beyond which the molecular anion is considered to be dissociated. $\tau(t_R)$ is the corresponding lifetime of the NIR. Assuming that the capture probability for each of the state is identical, one can estimate the forward backward asymmetry in the angular distribution using the potential energy curves of the two NIR states and their widths. As mentioned earlier, the relative amplitudes of each path will also depend on the lifetime of the individual NIR.

5.2. Angular distribution fits

Based on the model of coherent excitation of two resonances, we have analyzed the momentum images for the angular distributions, in an effort to quantify the relative contributions of the two resonances in the DEA signal and the relative phase, φ arising from the two dissociation paths. The angular distribution

clearly shows the contributions due to both Σ_g^+ and Σ_u^+ states. The functional form for the angular distribution under the above model is given by equation (7). The result of the fits is given in table 1. We find that the best fit values for the A_g and A_u do not provide a consistent picture as far as the relative intensities of the two channels are concerned. We believe that this is due to unsatisfactory resolution in the momentum imaging, the main contribution to which is the electron energy spread (about 0.6eV FWHM) and background noise, as seen above in the case of 4 eV resonance. Although, the best momentum resolution obtainable from the spectrometer used is about 10% (Δp/p), the relatively large width of the slice used (80nsec) in comparison with the overall time spread of the Newton sphere of ions (about 200 nsec) makes it worse. We have tried overcoming this effect by obtaining the angular distribution for the outermost edge of the image as explained earlier. Moreover, due to low cross section, a longer data acquisition time results in the substantial contribution from the background noise spoiling the contrast of the image. This highlights the need for better measurements using improved electron energy resolution.

Table 1. Relative amplitudes and phase from the angular distributions H^- from H_2 and D^- from D_2.

For H_2				For D_2			
Electron energy (eV)	A_g	A_u	φ(rad)	Electron energy (eV)	A_g	A_u	φ(rad)
14.5	0.36±0.06	0.78±0.04	4.3±0.08	14.0	0.48±0.03	0.87±0.02	4.70±0.03
15.0	0.26±0.08	0.81±0.04	4.0±0.24	14.5	0.40±0.15	1.06±0.09	4.53±0.13
15.5	0.21±0.08	0.73±0.04	3.14±0.05	15.0	0.68±0.02	0.67±0.04	4.58±0.03

Since reliable quantitative estimates of the relative amplitudes could not be obtained from the fits of the data, we use the integrated intensities in the forward and backward hemispheres of the images to obtain the forward-backward asymmetry factor, η defined as,

$$\eta = \frac{(I_{forward} - I_{backward})}{(I_{forward} + I_{backward})}. \quad (9)$$

The values of η are given in table 2 and are compared with the results of simulations described below.

Table 2. Forward-backward asymmetry factor obtained for H^- and D^- signal. (Reproduced from table 1 from reference 12).

H_2		D_{21}	
Electron energy (eV)	Asymmetry factor η	Electron energy (eV)	Asymmetry factor η
14.5	-0.19 ± 0.02	14.0	0.02 ± 0.02
15.0	-0.17 ± 0.02	14.5	-0.03 ± 0.02
15.5	-0.12 ± 0.02	15.0	-0.08 ± 0.02

5.3. Simulation of η using potential energy curves

Around 14eV, the electron scattering experiments have identified a NIR state with $^2\Sigma_g^+$ and estimated its width to be 90meV [31]. Taking the potential energy curve for this state from the literature [26] and assuming a potential energy curve that runs close to some of those available in this energy range we estimate the asymmetry factor η as

$$\eta = \frac{\sqrt{3}\exp\left[-\left(\frac{t_g}{2\tau_g}+\frac{t_u}{2\tau_u}\right)\right]}{\exp\left[-\left(\frac{t_g}{\tau_g}\right)\right]+\exp\left[-\left(\frac{t_u}{\tau_u}\right)\right]}\cos\varphi \quad (10)$$

where τ_g and τ_u are the average lifetimes of the Σ_g and Σ_u NIR states involved in DEA, t_g and t_u are the dissociation times for the parent anion along the respective potential energy curves for electron

attachment with a specified energy. The denominator of equation (10) is derived from using the cross section expression for DEA by each resonant state given by

$$\sigma_{DEA} = \sigma_c \times p_i \tag{11}$$

where the survival probability (p_i) for each resonant state is calculated using equation (8) and σ_c is the capture cross section. Although the width of the resonant states is strongly dependent on the inter-nuclear separation of the molecule, we have ignored this variation and replaced the lifetime with its average value over the dissociation path. We have also assumed that the two resonances show equal capture cross section at a given electron energy. This to some extent can be justified as the two potential energy curves considered for the simulations run very close to each other in the Frank-Condon region making their Franck-Condon factors almost equal for the transition from the vibrational and electronic ground state of the target. The numerator of equation (10) arises from the cross term of equation (7) integrated over the upper and lower half of space. The phase difference, φ, between the two paths is given by

$$\varphi = \frac{1}{\hbar}\int_{R_c}^{\infty}\left[\left(2\mathrm{m}\left(\mathrm{E}-\mathrm{V_u}(R)\right)\right)^{1/2} - \left(2\mathrm{m}\left(\mathrm{E}-\mathrm{V_g}(R)\right)\right)^{1/2}\right]\mathrm{d}R + \frac{\pi}{2} \tag{12}$$

where m is the reduced mass of the dissociating molecule, E is the electron energy and V(R) is the potential energy of the NIR states involved. The first term accounts for the phase difference arising from the two quantum paths of the dissociating wave packets. The additional phase of $\pi/2$ was obtained from the relative phase between the s and p partial waves of the plane wave description used for the incoming electron along the z-axis of the lab system. Ideally, in the presence of the target, the complex amplitudes of the partial waves will get distorted leading to an additional phase difference between the s and p waves, which will depend on the incident electron energy. However, as we use the zeroth order approximation, we have ignored this. We have taken the average lifetime for the $^2\Sigma_g^+$ state as 8fs based on its reported width and that for the $^2\Sigma_g^+$ as a parameter. The results obtained are shown in figure 3. The asymmetry factors are close to the observed values given in table 2.

As mentioned in the introduction, the symmetry of the NIR state active at 14eV was found to be a $^2\Sigma_g^+$ from electron scattering experiments [31]. On the other hand, the present angular distribution measurements of DEA indicate a strong contribution from the $^2\Sigma_u^+$ state. In fact, in the case of D_2 the slower dissociation results in greater loss of $^2\Sigma_g^+$ state amplitude to autodetachment, which makes the angular distribution more symmetric, dominated by the $^2\Sigma_u^+$ amplitude.

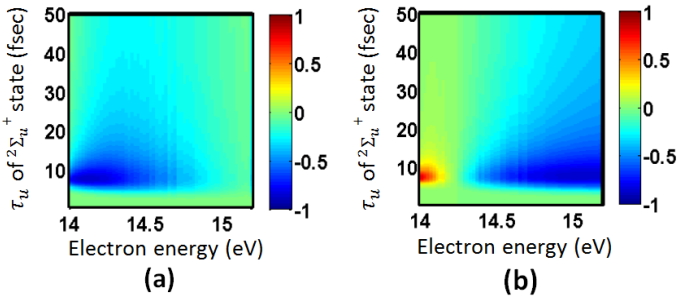

Figure 3. Estimated asymmetry factor as a function of electron energy and lifetime (τ_u) of the $^2\Sigma_u^+$ state in fsec for (a) H_2 and (b) D_2 where the lifetime of the $^2\Sigma_g^+$ state is taken as 8 fsec. (Reproduced from figure 4(b) and (d) of reference 12).

5.4. Signatures of quantum coherence in the scattered electron channel

We have seen above that the electron attachment process leads to a break in inversion symmetry at the 14 eV resonance due to coherent excitation of the two resonances of opposite parity. One would expect that the angular distribution of the autodetaching electrons from these resonances may also show corresponding asymmetry. It was the angular distribution of the ejected electrons at the incident energy of 14 eV that provided the identification of the symmetry of the resonance at this energy as $^2\Sigma_g^+$ [32]. However, a closer look at the data [32] shows a clear asymmetry in the angular distribution, which the authors acknowledged, but was left unexplained since a homonuclear diatomic molecule was expected

to provide a symmetric distribution. The limited angular range they used in the backward direction also did not help them.

5.5. Interferences in the ion yield curves

As discussed in Section 1, equally spaced structures in the ion yield curve from H_2 in the 14 eV resonance were observed earlier, while no such structures were observed in D_2 [30]. The measurements were performed at 90^0 with respect to the incoming electron beam. The observed oscillation in the ion signal was found to be at the interval of 0.2eV. It was argued that the spacing might correspond to the vibrational spacing of a $^2\Delta_g$ state, which was predissociating due to mixing with the $^2\Sigma_g^+$ NIR contributing to the DEA [30]. Since the difference in angular momenta of the two states is more than 1 unit, the mixing could happen only under breakdown of Born-Oppenheimer approximation. One may wonder if there is a connection with their observation and the present results.

We may conjecture whether the interference observed in the present experiment in terms of angular distribution gives rise to that observed in the ion yield curve at 90°. At $\theta = 90^o$, the interference term vanishes in the expression for $I(k, \theta)$ given above. So strictly, the interference that we observe could not have given rise to the oscillation in the ion yield curve. With the electron energy resolution of about 0.6 eV and reasonable imaging resolution ($\Delta p/p \sim 10\%$), we expect to observe the structures separated by 0.2 eV as reported by Tronc *et al.* [30] in the 90° direction. We are unable to see these structures, probably due to a large width of the time slice (80 nsec) in comparison with the overall time spread of the Newton sphere of ions (200nsec). Thus neither do we find a connection with those structures nor do we have an interpretation for it.

5.6. Lifetimes of resonances in coherent superposition

As can be seen from the logic of decay of a resonance, overlapping resonances with coherent excitation will not decay exponentially, although each of them shows exponential decay independently. Frishman and Shapiro have shown that such a superposition can be used to completely supress the decay of the resonance by suitably tweaking the relative phase between the two superposed states [36]. In light of this, it is interesting to see which way the coherent superposition of resonances affects the dynamics of the process. Our model, which gives reasonable match with the observed forward-backward asymmetry assumes that both the resonances retain their independent lifetime. That means they are understood to be decaying exponentially independent of one another. However, this is a crude approximation and it will be interesting to see a better model to describe the process.

6. Summary and conclusion

DEA to molecular hydrogen at the 14 eV resonance is found to be the result of coherent creation of two resonances of opposite parity leading to forward-backward asymmetry in the angular distribution of the fragment negative ion. As the wave packet propagates through two different paths based on the potential energy curves of the two resonances and leads to the same dissociation limit, we observe interference in the forward-backward asymmetry factor as a function of the electron energy. This interference is also dependent on the isotopic composition as seen in the case of D_2. Simulation using model potential energy curves shows fair agreement with the observed asymmetry. Fitting the angular distribution data as a function of electron energy using $^2\Sigma_g^+$ and $^2\Sigma_u^+$ symmetries qualitatively shows the contributions from both resonances. However, due to limited momentum resolution, quantitative estimates of the amplitudes of the two resonances could not be obtained with any reliability. We do not observe any signatures of the structures seen in an earlier report in the ion yield curves around 14 eV. It is clear that further experimental and theoretical work on NIR states are needed even for the simplest molecule.

Acknowledgement

E.K. acknowledges a Marie Curie Fellowship during the course of the measurements and Raja Ramanna Fellowship, Department of Atomic Energy India. V.S.P. acknowledges the Department of Atomic Energy, India for financial support. N.J.M. recognizes support from the European Union Framework 7

programme LASSIE Marie Curie ITN Grant Agreement 238258 and VAMDC INFRA-2008-1.2.2 Scientific Data Infrastructure. Grant Agreement no.: 239108.

References

[1] Prabhudesai V S, Kelkar A H, Nandi D and Krishnakumar E 2005 *Phys. Rev. Lett.* **95** 143202
[2] Prabhudesai V S, Nandi D, Kelkar A H and Krishnakumar E 2008 *J. Chem. Phys.* **128** 154309
[3] Ptasinska S *et al.* 2005 *Phys. Rev. Lett.* **95** 093201
[4] Ibănescu B C and Allan M 2009 *Phys. Chem. Chem. Phys.* **11** 7640
[5] Samukawa S 2005 *Japan. J. Appl. Phys.* **45** 2395
[6] Sansone G *et al.* 2010 *Nature* **465** 763
[7] Krishnakumar E and Nagesha K 1992 *J. Phys.* B*: At. Mol. Opt. Phys.* **25** 1645
[8] Rawat P *et al.* 2007 *J. Phys.* B*: At. Mol. Opt. Phys.* **40** 4625
[9] Rawat P *et al.* 2008 *Int. J. of Mass Spectrom*. **277**, 96
[10] Krishnakumar E and Prabhudesai V S 2019 *Springer Proc. In Phys.* **230** 20
[11] Fabrikant I I, Eden S, Mason N J and Fedor J 2017 *Adv. Atom. Mol. Opt. Phys.* **66** 545
[12] Krishnakumar E, Prabhudesai V S and Mason N J 2018 *Nat. Phys.* **14** 149
[13] Christophorou L G, McCorkle D L and Christodoulides A A 1984 *Electron-Molecule Interactions and Their Applications* vol 1 ed Christophrous L G (New York: Academic) ch 6
[14] Yoon J-S *et al.* 2008 *J. Phys. Chem. Ref. Data* **37** 913
[15] Yoon J-S *et al.* 2010 *Rep. Prog. Phys.* **73** 116401
[16] Schulz G J 1973 *Rev. Mod. Phys.* **45** 423
[17] Zecca A, Karwasz G P and Brusa R S 1996 *La Rivista del Nuovo Cimento* **19** 1
[18] Krishnakumar E, Denifl S, Čadež I, Markelj S and Mason N J 2011 *Phys. Rev. Lett*. **106**, 243201
[19] Schulz G J 1959 *Phys. Rev. Lett.* **113** 816
[20] Rapp D, Sharp T E and Briglia D D 1965 *Phys. Rev. Lett.* **14** 533
[21] Schulz G J and Asundi R K 1967 *Phys. Rev.* **158** 25
[22] Fedor J, Kočišek J and Janečková R 2015 *J. Phys.: Conf. Ser.* **635** 072093
[23] Allan M and Wong S F 1978 *Phys. Rev. Lett.* **41**, 1791
[24] Čadež I *et al.* 1988 *J. Phys.* B*: At. Mol. Opt. Phys.* **21** 3271
[25] Celiberto R *et al.* 2011 *Atom. Data Nucl. Data Tables* **77** 161
[26] Fabrikant I I, Wadehra J M and Xu Y 2002 *Phys. Scr.* **2002** 45
[27] Sharp T E 1971 *Atom. Data Nucl. Data Tables* **2** 119
[28] Eliezier I, Taylor H S and Williams Jr J K 1967 *J. Chem. Phys.* **47** 2165
[29] Stibbe D T and Tennyson J 1998 *J. Phys.* B*: At. Mol. Opt. Phys.* **31** 815
[30] Tronc M, Hall R I, Schermann C and Taylor H S 1979 *J. Phys.* B*: At. Molec. Phys.* **12** L279
[31] Tronc M, Fiquet-Fayard F, Schermann C and Hall R I 1977 *J. Phys.* B*: At. Molec. Phys.* **10** 305
[32] Weingartshofer A, Ehrhardt H, Hermann V and Linder F 1970 *Phys. Rev*. A **2** 204
[33] O'Malley T F 1966 *Phys. Rev.* **150** 14
[34] Nandi D, Prabhudesai V S, Krishnakumar E and Chatterjee A 2005 *Rev. Sci. Instrum.* **76** 053107
[35] O'Malley T F and Taylor H S 1968 *Phys. Rev.* **176** 207
[36] Frishman E and Shapiro M 2001 *Phys. Rev. Lett.* **87** 253001